Improvement in IBC-silicon solar cell performance by insertion of highly doped crystalline layer at heterojunction interfaces

Hadi Bashiri, Mohammad Azim Karami†, and Shahramm Mohammadnejad

School of Electrical Engineering, Iran University of Science &Technology (IUST), Narmak, Tehran 16844, *Iran*

(Received 27 April 2017; revised manuscript received 13 June 2017; published online 20 August 2017)

By inserting a thin highly doped crystalline silicon layer between the base region and amorphous silicon layer in an interdigitated back-contact (IBC) silicon solar cell, a new passivation layer is investigated. The passivation layer performance is characterized by numerical simulations. Moreover, the dependence of the output parameters of the solar cell on the additional layer parameters (doping concentration and thickness) is studied. By optimizing the additional passivation layer in terms of doping concentration and thickness, the power conversion efficiency could be improved by a factor of 2.5%, open circuit voltage is increased by 30 mV and the fill factor of the solar cell by 7.4%. The performance enhancement is achieved due to the decrease of recombination rate, a decrease in solar cell resistivity and improvement of field effect passivation at heterojunction interface. The above-mentioned results are compared with reported results of the same conventional interdigitated back-contact silicon solar cell structure. Furthermore, the effect of a-Si:H/c-Si interface defect density on IBC silicon solar cell parameters with a new passivation layer is studied. The additional passivation layer also reduces the sensitivity of output parameter of solar cell to interface defect density.

Keywords: IBC silicon solar cells, interface layer, recombination, interface defect density

PACS: 88.40.fc, 88.40.hj, 88.40.jj, 85.60.Bt **DOI:** 10.1088/1674-1056/26/10/108801

1. Introduction

Interdigitated back-contact (IBC) silicon solar cells were introduced to maximize the open circuit voltage (V_{oc}) of the solar cell, by eliminating the shadow effect of electrodes at the front surface while reducing the series resistance.[1] An improvement in IBC silicon solar cell performance is achieved when a thin layer of a-Si:H was used as a passivation layer and interdigitated back-contact silicon heterojunction (IBC-SHJ) solar cells were investigated.[2] IBC-SHJ solar cells are able to produce high V_{oc} and low recombination rate at the surface due to heterojunction contacts. Deposition of a-Si:H layer on the crystalline silicon substrate is a low-temperature process (less than 200 °C) which possesses many advantages such as a better control to define p-type and n-type regions, preventing the wafer from wrapping and cracking and efficient passivation of c-Si wafer surface.[2] By the use of plasma-enhanced chemical vapor deposition (PECVD), a high-quality a-Si:H layer on the crystalline silicon wafer with an effective surface recombination velocity (SRV) of less than 6.2 cm/s was reported.[3] In recent years, many research studies were conducted to improve the electrical characteristics and achieve the maximum efficiency of IBC-SHJ solar cells.[4–9] A thin layer of intrinsic a-Si:H was added to the back surface of the solar cell, and increases in V_{oc} and short circuit current (J_{sc}) were observed.[4,5] It was also concluded that by reducing the buffer layer thickness, reducing the buffer layer bandgap and increasing the conductivity of buffer layer, a better fill factor was achieved.[4,5] Padilla *et al.* used a photoluminescence images-based technique to characterize recombination rate at the surface of IBC-SHJ solar cells.[6] Interface defects were identified as one of the most important factors limiting the heterojunction solar cell performance. High-quality passivation layer was used to solve the interface defect problem.[7–9] In their study a thin (< 10 nm) layer of (n^+) c-Si:H was deposited on p-type c-Si substrate by PECVD. The layer was used as an interlayer emitter in back-contact heterojunction structure. The high electric field provided by (n^+) c-Si:H reduces the recombination rate of minority carriers at emitter surface, and 0.7% increase in efficiency compared with the efficiency of conventional HIT was reported. The reduction in recombination rate by producing a high electric field is named field effect passivation.[10] Moreover, by combining two types of homojunction and heterojunction, homo-heterojunction (HHJ) concept was proposed.[11] With this combination, higher fill factor (FF) than that of conventional HIT was obtained due to a reduction in series resistance, also the sensitivity of output parameters to the density of states (DOS) was reduced due to field effect passivation.[11] Recently an HIT structure was reported to improve back-contacted silicon solar cell performance with a focus on the reduction of recombination at heterointerfaces. It was shown that by depositing a thin (n^+) buffer layer on the p-type substrate and preserving (i) a-Si:H layer V_{oc} increases and the sensitivity of output parameter to DOS decreases.[12] Figure 1 shows the HET cell with buffer layers at the front and back surfaces. In this study, the field effect passivation of interface defect density through using the

†Corresponding author. E-mail: karami@iust.ac.ir

© 2017 Chinese Physical Society and IOP Publishing Ltd

electric field effect provided by thin highly doped buffer layer in IBC-SHJ solar cell is proposed. Also the reduction of surface recombination at IBC-SHJ solar cell interfaces, by using the buffer layer and HHJ concept in IBC-SHJ structure is studied. Starting from standard n-type IBC-SHJ architecture reported in Ref. [13] and reproducing the experimental result by numerical simulations, HHJ-IBC-SHJ architecture is investigated by inserting the highly doped c-Si layer. In Section 2 the theory of recombination at heterojunction interfaces is established, while in Section 3, the numerical modeling of the proposed structure is presented. In Section 4 the simulation results and discussion are presented.

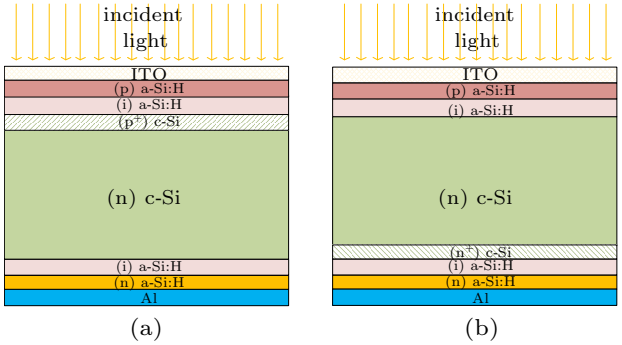


Fig. 1. (color online) Cross sections of HET cells, cross sections having HHJ architectures with (a) the inserted (p^+p) c-Si or/and (b) (n^+p) c-Si layers.

2. Heterojunction interface recombination modeling

It was suggested that the recombination model used in amphoteric structures can be extended to modelling the recombination at c-Si/a-Si:H interface.[14,15] Although the mentioned model can be used in solar cells in specific operating conditions, the recombination at c-Si/a-Si:H interface can be modeled by considering a hypothetical thin layer of defect state at c-Si/a-Si:H interface where the amorphous layer specification is applied.[16] This layer has two mid-gap dangling bands: donor-like and acceptor-like, with two Gaussian distribution functions, a conduction band tail, and a valance band tail that is shown in Fig. 2. In this study, an extended formalism of Shockley–Read–Hall (SRH) theory[17,18] is used for recombination calculation at heterojunction interface. The net recombination rates for electrons and holes in steady state condition are given by[19]

$$
\begin{aligned}
R_n = R_p = \int_{E_V}^{E_C} \Bigg(& \frac{v_n v_p \sigma_{tae} \sigma_{tah} \left(np - n_i^2\right) g_{TA}(E)}{v_n \sigma_{tae} \left(n + n_i e^{\frac{E-E_i}{kT}}\right) + v_p \sigma_{tah} \left(p + n_i e^{\frac{E_i-E}{kT}}\right)} \\
& + \frac{v_n v_p \sigma_{gae} \sigma_{gah} \left(np - n_i^2\right) g_{GA}(E)}{v_n \sigma_{gae} \left(n + n_i e^{\frac{E-E_i}{kT}}\right) + v_p \sigma_{gah} \left(p + n_i e^{\frac{E_i-E}{kT}}\right)} \\
& + \frac{v_n v_m v_p \sigma_{tde} \sigma_{tah} \left(np - n_i^2\right) g_{TD}(E)}{v_n \sigma_{tde} \left(n + n_i e^{\frac{E-E_i}{kT}}\right) + v_p \sigma_{tdh} \left(p + n_i e^{\frac{E_i-E}{kT}}\right)} \\
& + \frac{v_n v_p \sigma_{gde} \sigma_{tah} \left(np - n_i^2\right) g_{GD}(E)}{v_n \sigma_{tde} \left(n + n_i e^{\frac{E-E_i}{kT}}\right) + v_p \sigma_{tdh} \left(p + n_i e^{\frac{E_i-E}{kT}}\right)} \Bigg), \quad (1)
\end{aligned}
$$

where E_V and E_C are the valance and conduction band energy levels respectively, v_n and v_p are the electron and hole surface recombination velocity, σ_{tae} and σ_{tde} are the band tail acceptor-like and donor-like capture cross section respectively, σ_{gae} and σ_{gah} are the mid-gap Gaussian state acceptor-like and donor-like capture cross section respectively, $g_{TA}(E)$ and $g_{GA}(E)$ are the tail and Gaussian defect DOS respectively.

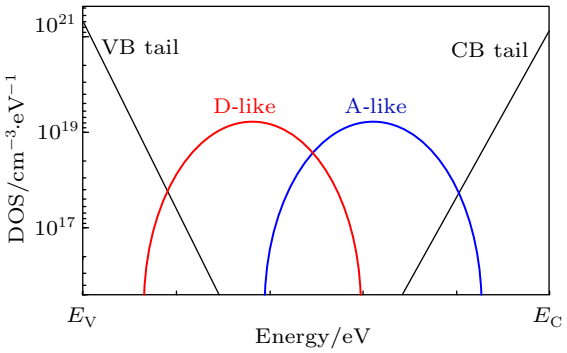


Fig. 2. (color online) DOS distributions in a-Si and interface defect layers.

3. Simulation models

Figure 3 shows a schematic diagram of IBC-SHJ solar cell studied in Ref. [13]. The device consists of 150-μm n-type float zone (FZ) c-Si substrate with a phosphorous doping

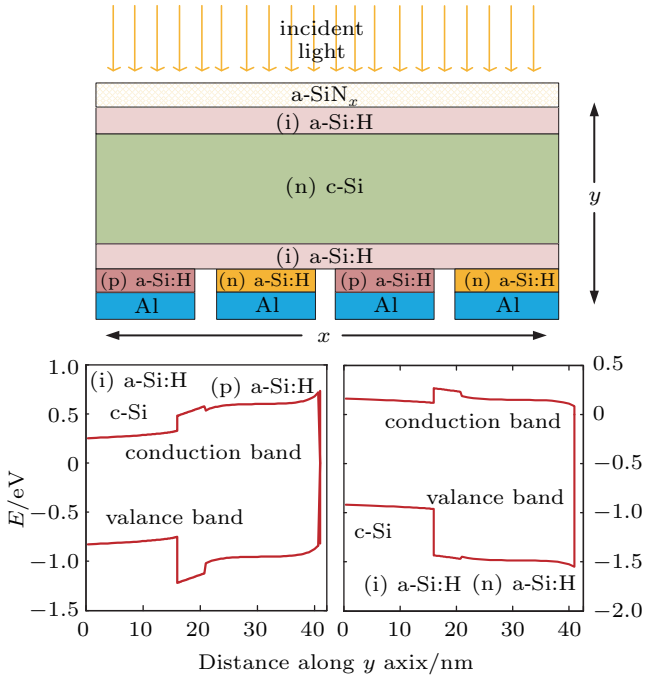


Fig. 3. (color online) The schematic and band diagrams of IBC-SHJ solar cell simulation model.

concentration of 2×10^{15} cm^{-3}, a 5-nm (i) a-Si:H layer as a front surface passivation layer, 60-nm a-SiN$_x$:H layer anti-reflection coating. Moreover, on the back side of the cell, a thin layer of (i) a-Si:H layer with a thickness of 5 nm is deposited as a passivation layer. A 20-nm thick (p) a-Si:H layer as emitter contact and a 20-nm thick (n) a-Si:H layer as base contacts are the next layers to be deposited on the back surface (i) a-Si:H layer. The lateral dimensions of each pair of emitter and base contacts and also the gap between them are 240 μm and 125 μm, and 25 μm respectively. The device modeling is performed with a commercial device simulator[20] under a standard beam intensity of 1000 W/cm^{-2}. The ray tracing method is used to analyze the optical paths through the device. To describe the carrier transport through c-Si and all amorphous layers, the conventional drift-diffusion model is used. The SRH and Auger model is coupled to the simulator to describe the recombination. To describe carrier transport at heterojunction interface, Fowler–Nordheim, thermionic tunnel, and trap assisted tunnel model are used. Moreover, to describe mobility across region with a high doping concentration, the concentration mobility-dependent model is utilized. Defect state at a-Si:H/c-Si heterojunction, is modeled with a thin ($d_{\rm int} = 1$ nm) defect layer that should be defined at a-Si:H/c-Si heterojunction.[19] In this layer, both the donor- and acceptor-like defects with Gaussian distribution are placed in the band gap.[21] Interface-defect density $D_{\rm it}$ (cm$^{-2} \cdot$eV^{-1}) is determined according to

$$D_{\rm it} = g_{\rm it} \times d_{\rm int}, \tag{2}$$

where $g_{\rm it}$ is the density of state (DOS) and $d_{\rm int}$ is the thickness of defective layer.[21,22] For the IBC-SHJ solar cell simulation, the physical parameters that are listed in Table 2 according to Ref. [13] are used. Minority carrier lifetime in the c-Si is considered as 1 ms. For all a-Si:H layers the electron and hole surface recombination velocity is $v_{\rm surfn} = v_{\rm surfp} = 80$ cm/s, and the carrier mobility values are considered to be 10 cm^2·s/V and 1 cm^2·s/V for electrons and holes respectively.[13]

Table 1. Recombination parameters at heterojunction interfaces.

Interface	$D_{\rm it}$/cm^{-2}·eV^{-1}	σ_n/cm^2	σ_p/cm^2
(i) a-Si:H/c-Si (p-type)	3.1×10^{11}	8×10^{-18}	2×10^{-15}
(i) a-Si:H/c-Si (gap)	1.7×10^{11}	5×10^{-16}	5×10^{-16}
(i) a-Si:H/c-Si (n-type)	1.6×10^{11}	1×10^{-18}	3×10^{-16}
(i) a-Si:H/c-Si (front)	4.4×10^{10}	3×10^{-18}	6×10^{-17}

Table 2. DOS distributions for a-Si:H layers.

Material		c-Si	(i) a-Si:H	(n) a-Si:H	(p) a-Si:H
Doping concentration/cm^{-3}		2×10^{15} (phosphorus)	2.2×10^{15} (phosphorus)	1.2×10^{19} (phosphorus)	2×10^{19} (boron)
Electron affinity χ/eV		4.05	3.9	3.9	3.9
Bandgap $E_{\rm g}$/eV		1.12	front layer 1.8 back layer 1.7	1.72	1.65
Conduction tail states	NTA/cm^{-3}	–	1×10^{18}	1×10^{21}	1×10^{21}
	ETA/eV	–	0.04	0.07	0.07
	σ_N/cm^2	–	7×10^{-17}	1×10^{-16}	1×10^{-16}
	$\sigma_{\rm C}$/cm^2	–	7×10^{-15}	1×10^{-16}	1×10^{-16}
Valance tail states	NTD/cm^{-3}	–	1×10^{18}	1×10^{21}	1×10^{21}
	ETD/eV	–	0.06	0.12	0.12
	σ_N/cm^2	–	7×10^{-17}	1×10^{-16}	1×10^{-16}
	$\sigma_{\rm C}$/cm^2	–	7×10^{-15}	1×10^{-16}	1×10^{-16}
Donor-like Dangling bond-states	NGD/cm^{-3}	–	1×10^{16}	1.5×10^{19}	1.5×10^{19}
	EGD/eV	–	0.9	0.45	1.1
	WGD/eV	–	0.15	0.2	0.2
	σ_N/cm^2	–	2×10^{-15}	5×10^{-15}	5×10^{-15}
	$\sigma_{\rm C}$/cm^2	–	2×10^{-14}	5×10^{-14}	5×10^{-14}
Acceptor-like Dangling bond-states	NGA/cm^{-3}	–	1×10^{16} cm^{-3}	1.5×10^{19}	1.5×10^{19}
	EGA/eV	–	1.1 eV	0.7	1.3
	WGA/eV	–	0.15 eV	0.2	0.2
	σ_N/cm^2	–	2×10^{-15}	5×10^{-15}	5×10^{-15}
	$\sigma_{\rm C}$/cm^2	–	2×10^{-14}	5×10^{-14}	5×10^{-14}

4. Results and discussion

4.1. Comparison of solar cell performance

To evaluate the accuracy of the simulation, current–voltage (JV) curve of the IBC-SHJ solar cell is simulated and compared with the baseline experimental devices fabricated in Ref. [13], as shown in Fig. 4(a). It can be seen that $J_{\rm sc}$, $V_{\rm oc}$, FF, and efficiency are well matched. Also in Fig. 4(b), the IBC-SHJ solar cell efficiency as a function of $D_{\rm it}$ value at the gap region heterojunction interface is simulated and compared with the simulation result in Ref. [13]. The comparison of effi-

ciency changing with D_{it} shows that the simulation results and the current simulation results in Ref. [13] are in good agreement.

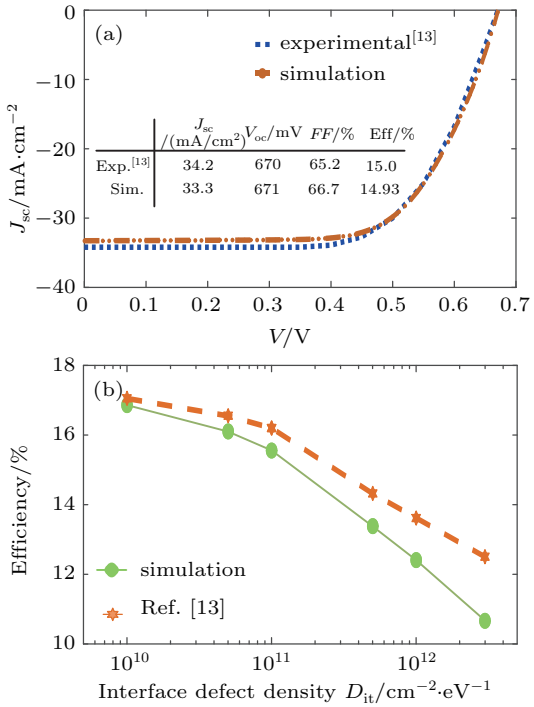


Fig. 4. (color online) (a) *JV* curve of IBC-SHJ solar cells and (b) effect of D_{it} at (i) a-Si:H/c-Si interface close to gap region on IBC-SHJ solar cell parameters.

4.2. Highly doped crystalline layer at front surface and back surface

In this section, the effect of heterojunction interface defects on the IBC-SHJ solar cell performance in the presence of a thin and highly doped buffer layer is studied. The effect of the (p^+) c-Si buffer layer on each surface is studied independently. In Figs. 5(a) and 5(b), the IBC-SHJ solar cells with HHJ structure at the front surface and the back surface are shown respectively. In the first structure (front surface HHJ-IBC), the doping concentration of (p^+) c-Si buffer layer is assumed to be 5×10^{18} cm^{-3} and the layer thickness is assumed to be 20 nm.

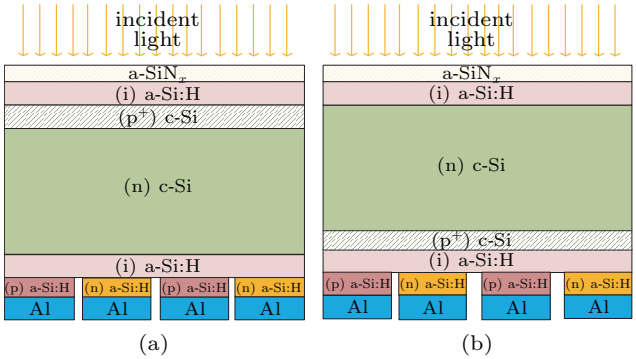


Fig. 5. (color online) Cross sections of (a) front surface HHJ-IBC and (b) back surface HHJ-IBC.

In the simulation model, all physical parameters listed in Tables 1 and 2 are used. Doping concentration of thin interface layer (1 nm) that is used to describe the defects existing in crystal and amorphous layer is the same as the (p^+) c-Si layer. Figure 6 shows the effects of the (p^+) c-Si buffer layer on front surface IBC-SHJ solar cell parameters when the interface defect density at a-Si:H/(p^+) c-Si layer increases from 1×10^{10} cm^{-3}·eV^{-1} to 3×10^{12} cm^{-3}·eV^{-1}. The simulation results show that D_{it} increasing to 1×10^{12} cm^{-3}·eV^{-1} does not show any significant effect on front surface IBC-SHJ solar cell parameters while in conventional IBC for D_{it} 1×10^{12} cm^{-3}·eV^{-1}, J_{sc}, V_{oc}, and efficiency, 8 mA, 150 mV, and 3.5% are reduced respectively and FF is increased by 1%. Therefore, the sensitivity of the front surface HHJ-IBC solar cell parameter is reduced to D_{it} due to the reduction in recombination rate. In the next step, the effect of D_{it} on back surface HHJ-IBC performance is studied and compared with the scenario of conventional IBC solar cell. Doping concentration and thickness of (p^+) c-Si buffer layer as well as front surface are considered to be 5×10^{18} cm^{-3} and 20 nm respectively. It is assumed that the values of D_{it} at a-Si:H/(p^+) c-Si interface for p-region, and n-region are constant and only the value of D_{it} in the gap region is changed for the simulation simplicity. The simulation results are plotted in Fig. 7, showing that by adding (p^+) the c-Si the sensitivity of back surface HHJ-IBC parameters is reduced. The reduction in recombination rate at a-Si:H/(p^+) c-Si is the most important reason for justifying this manner.

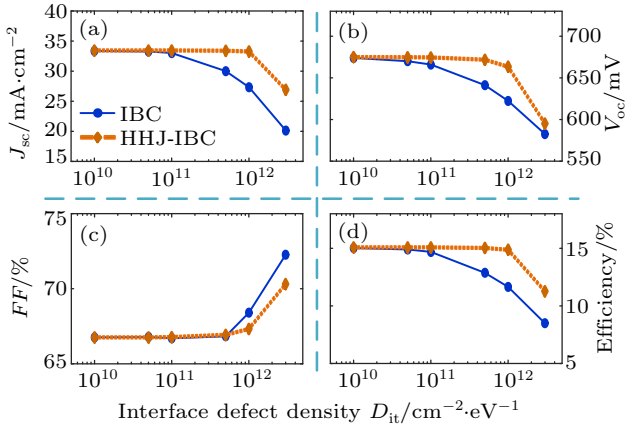


Fig. 6. (color online) Effects of (p^+) c-Si buffer layer on the performance parameters of front surface HHJ-IBC.

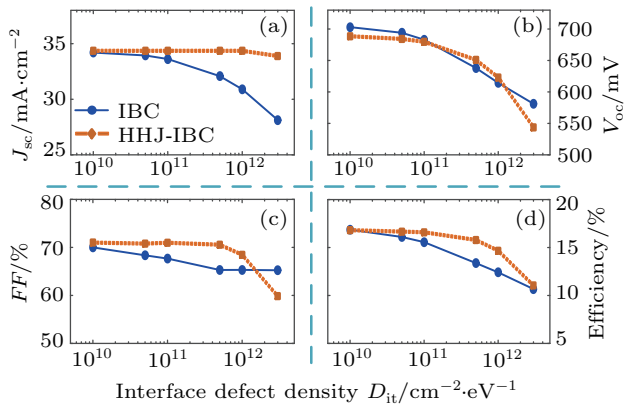


Fig. 7. (color online) Effects of (p^+) c-Si buffer layer on output parameters of back surface HHJ-IBC.

4.3. Discussion

The simulation results show that the performance of the IBC-SHJ solar cells is limited by the a-Si:H/c-Si properties (band offset, interface defect,...). Interface-defect density plays a critical role in the solar cell parameters, acting as the recombination centers. Furthermore, defect states change the charge neutrality at crystalline silicon interface with trapping free charges (electrons or holes). Interface-defect can strongly reduce the V_{oc}, as the number of trapped carriers increases, the band diagram of energy bends, and the value of Φ_B decreases,. Hence finding a solution to overcome the interface-defects can help to improve the solar cell performance. As seen in Figs. 6 and 7 in the case of the IBC-SHJ solar cells with additional layer, electrical current loss occurs at a slower rate than in the case of conventional IBC-SHJ. This can be attributed to a reduction in recombination rate at the a-Si:H/c-Si interface.

Figure 8(a) shows the recombination rate at c-Si/(i)a-Si:H/(p)a-Si:H interface and figure 8(b) shows the recombination rate at c-Si/(i)a-Si:H/(n)a-Si:H interface on the back surface of IBC-SHJ solar cell, which are plotted according to Eq. (1) for both cases, i.e., with and without the (p^+) c-Si buffer layer. It is obvious that adding (p^+) c-Si buffer layer reduces the recombination rate at interface. By comparing the voltage drops for the two cases of IBC-SHJ solar cells with and without (p^+) c-Si buffer layer in Figs. 6 and 7, it is observed that as the number of defects at the interface increases the voltage drop is less in the case of IBC-SHJ solar cell with the (p^+) c-Si buffer layer. Any change in the recombination rate at the c-Si /a-Si:H interface directly affects the open circuit voltage:[23]

$$V_{oc} = \frac{\Phi_B}{q} - \frac{kT}{q} \ln\left(\frac{qN_V U_{it}}{j_{SC}\Delta n}\right), \tag{3}$$

where U_{it} is the total recombination rate at heterojunction interface, Φ_B the potential barrier height, Δn the carrier concentration, q the electron charge, and N_V the effective density of state in valance band energy. From Eq. (3) it follows that by reducing the recombination rate and increasing the Φ_B, the V_{oc} increases. Interface defects change the electrical field at the heterojunction interface and carrier inversion. Hence the increase of interface defect number leads to further bending energy bands, and reducing Φ_B. In addition, a thin (p^+) c-Si buffer layer modifies the band offset at the interface.

Figure 9 shows energy band diagrams on both emitter and base side for IBC-SHJ solar cell with and without (p^+) c-Si buffer layer, adding (p^+) c-Si buffer layer leads to Fermi level shifting toward the valence band and field effect passivation improvement at (p^+) c-Si buffer layer where the negative effect of D_{it} is suppressed. According to Eq. (3), the increase of effective barrier height and the decrease of recombination at interface can improve the open circuit voltage. Therefore V_{oc} is less sensitive to D_{it}. By comparing the obtained result for FF in Figs. 6 and 7, it is observed that adding (p^+) c-Si buffer layer leads to a better result, because (p^+) c-Si buffer layer enhances carrier transport at c-Si/(i)a-Si:H interface, which leads to higher FF.

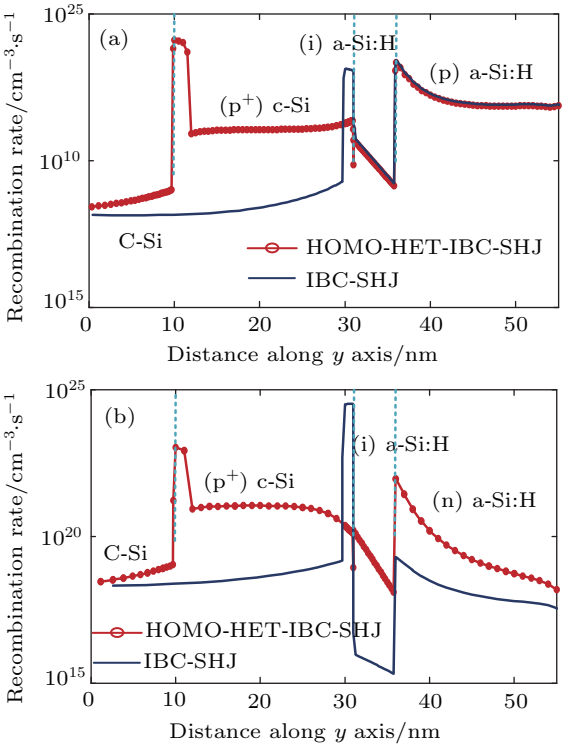


Fig. 8. (color online) Recombination rates at (a) front surface and (b) back surface each as a function of position at a-Si:H/c-Si interface for conventional IBC-SHJ and IBC-SHJ with (p^+) c-Si buffer layer.

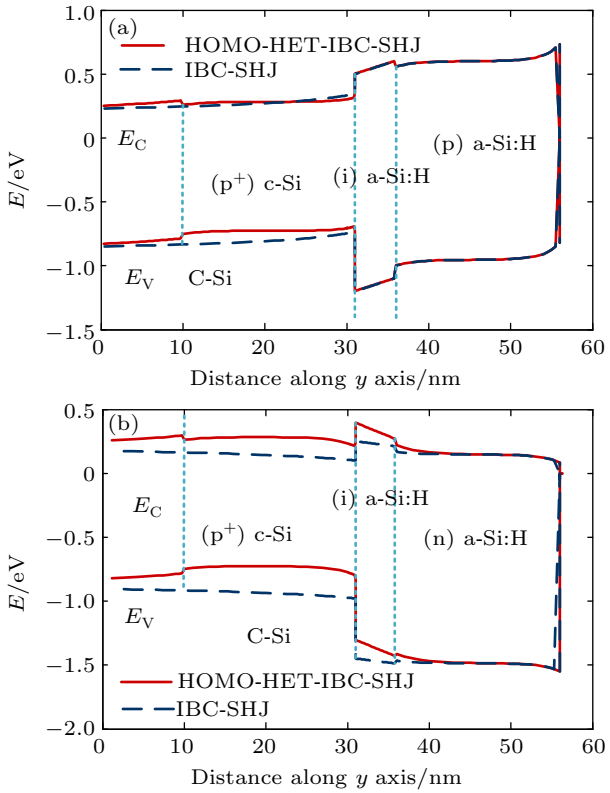


Fig. 9. (color online) Band diagrams of the conventional IBC-SHJ and IBC-SHJ with (p^+) c-Si buffer layer cells with the added layers at (a) emitter side interface and (b) base side interface.

4.4. Optimization of highly doped crystalline layer

In this subsection, the two (p^+) c-Si buffer layers respectively at the front surface and the back surface of IBC-SHJ solar cell substrate are optimized in two terms of layer thickness and doping concentration to achieve the maximum conversion efficiency. For this purpose, in the first step, the numerical simulation is used for optimizing the front surface (p^+) c-Si buffer layer, and then the back surface (p^+) c-Si buffer layer is optimized. All material parameters listed in Table 1 and the interface layer properties listed in Table 2 are used for simulation. To find the optimum thickness of (p^+) c-Si buffer layer, doping concentration of the layer is kept constantly at 1×10^{18} cm^{-3} and thickness changes from 1 nm to 100 nm.

Figure 10(a) shows IBC-SHJ solar cell parameter, i.e., efficiency as a function of the front surface (p^+) c-Si buffer layer thickness. It is clear that the best performance for the solar cell can be achieved when the thickness of (p^+) c-Si buffer layer is higher than 10 nm.

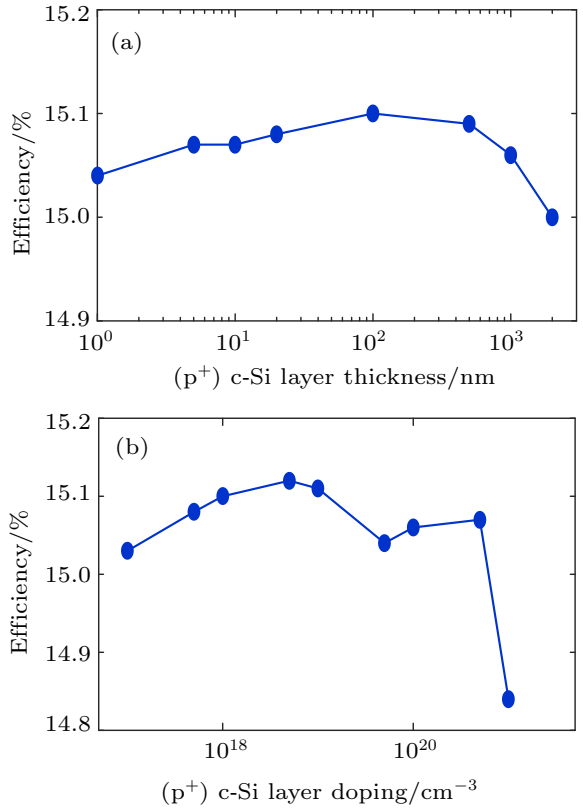


Fig. 10. (color online) IBC-SHJ solar cell overall efficiencies versus (a) front surface (p^+) c-Si buffer layer thickness and (b) front surface (p^+) c-Si buffer layer doping concentration respectively.

Figure 10(b) shows the solar cell parameter, i.e., efficiency versus doping concentration of front surface (p^+) c-Si buffer, where the thickness of the layer is kept constantly at 10 nm. The results show that the best performance of the cell can be achieved when doping concentration of the layer is 5×10^{18} cm^{-3}. For optimizing the back surface (p^+) c-Si buffer layer, a front surface (p^+) c-Si buffer layer with 10 nm thickness and 5×10^{20} cm^{-3} doping concentration is considered, then with adding a 20-nm (p^+) c-Si buffer layer to the back surface of the IBC-SHJ solar cell, and varying the doping concentration of the layer from 1×10^{17} cm^{-3} to 1×10^{21} cm^{-3}, the optimum doping concentration of the layer is calculated.

Figure 11(a) shows the overall conversion efficiency of the cell versus back surface (p^+) c-Si buffer layer thickness, where the maximum efficiency is achieved when the thickness is between 10 nm and 30 nm. Figure 11(b) shows the effect of the layer doping concentration on the cell overall conversion efficiency. As seen from the figure, the maximum efficiency of the cell is obtained when doping concentration is approximately 1×10^{19} cm^{-3}. In the same way, the optimum back surface (p^+) c-Si buffer layer thickness is obtained, when doping concentration of the layer is kept constantly at 1×10^{19} cm^{-3} and then with varying the thickness of the layer from 1 nm to 100 nm, the optimum thickness is obtained.

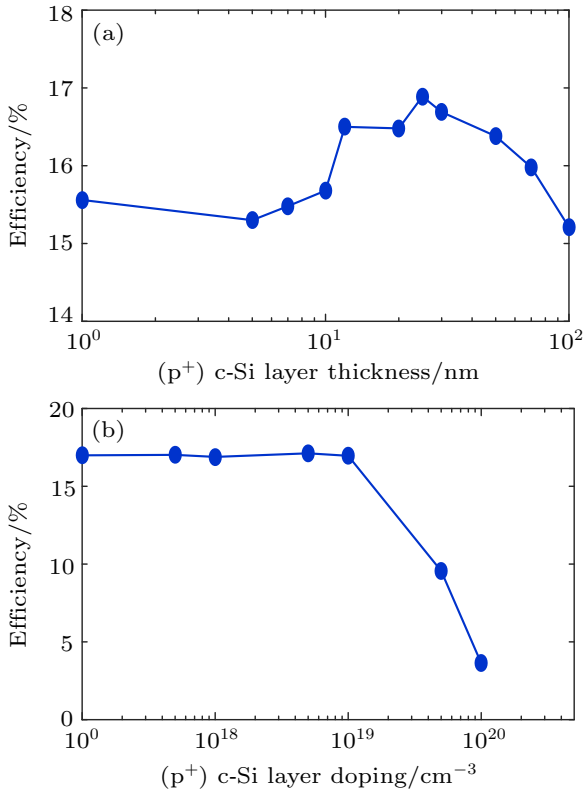
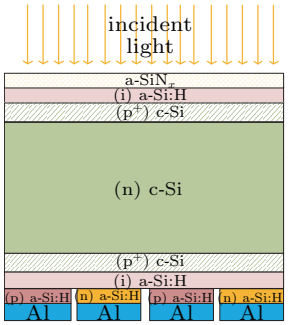


Fig. 11. (color online) IBC-SHJ solar cell overall efficiencies versus (a) back surface (p^+) c-Si buffer layer thickness and (b) back surface (p^+) c-Si buffer layer doping concentration, respectively.

Figure 12 shows the final structure of HHJ-IBC-SHJ silicon solar cell with two added (p^+) c-Si buffer layers respectively at the front surface and the back surface of substrate, also a comparison with reported result in Ref. [13] is performed. It can be found that about 2.5% increase in efficiency is achievable with the investigated structure compared with conventional IBC-SHJ silicon solar cell.



	Ref. [13]	HHJ-IBC-SHJ
$J_{sc}/(mV/cm^2)$	34.2	34.4
V_{oc}/mV	670	700
$FF/\%$	65.2	72.6
Efficiency/%	15.0	17.55

Fig. 12. (color online) Final structure of HHJ-IBC-SHJ silicon solar cell with two added (p^+) c-Si buffer layers respectively at the front surface and the back surface of the substrate.

5. Conclusions

In this paper, an IBC-SHJ solar cell with a modified structure is presented. By inserting a thin and highly doped layer of c-Si between the front and back surfaces of the solar cell substrate, an HHJ-IBC-SHJ structure is investigated. In the new structure, the electrical field at heterojunction interface is improved and a passivation layer is formed at the c-Si substrate surface. The added layer reduces the recombination rate at the heterojunction interface and the solar cell output parameter is improved. Furthermore, the sensitivity of the solar cell parameter to interface defect density is reduced. Finally, the optimization of the added layer is performed in terms of doping concentration and thickness. Considering the doping concentration of 5×10^{18} cm^{-3} and 100-nm thick for the upper layer and the doping concentration of 5×10^{18} cm^{-3} and 25-nm thick for the lower layer, the maximum increase in the IBC-SHJ solar cell efficiency is achieved to be about 2.5%.

References

[1] Schwartz R J and Lammert M D 1977 *IEEE Trans. Electron Dev.* **24** 337

[2] Lu M, Bowden S, Das U and Birkmire R 2007 *Appl. Phys. Lett.* **91** 063507

[3] Shu B, Das U, Appel J, McCandless B and Hegedus S and Birkmire R 2010 *Proceedings of the 35th IEEE Photovoltaic Specialist Conference*, June 20–25, 2010, Honolulu, USA, p. 003223

[4] Lu M, Das U, Bowden S, Hegedus S and Birkmire R 2009 *34th IEEE Photovoltaic Specialists Conference*, June 7–12, 2009, Philadelphia, USA, p. 1475

[5] Diouf D, Kleider J P, Desrues T and Ribeyron P J 2009 *Mater. Sci. Eng. B* **159–160** 291

[6] Padilla M, Höffler H, Reichel C, H. Chu, Greulich J, Rein S, Warta W, Hermle M and Schubert M C 2014 *Solar Energy Mater. Solar Cells* **120** Part A363

[7] Schmidt M, Korte L, Laades A, Stangl R, Schubert C, Angermann M S H, Conrad E and Maydell K V 2007 *Thin Solid Films* **515** 7475

[8] Angermann M S H, Schulze T F, Conrad E, Rappich J and Korte L 2008 *Proceedings of 23rd European Photovoltaic Solar Energy Conference*, September 1–5, September 2008 (Val. Spain, 2008), p. 1422–1426

[9] Xiao S and Xu S 2014 *Crit. Rev. Solid State Mater. Sci.* **39** 277

[10] Hekmatshoar B, Shahrjerdi D and Sadana D K 2011 *IEEE International Electron Devices Meeting*, December 5–7, 2011, Washington, DC, USA (IEEE, 2011), p. 36-6

[11] Zhong S, Hua X and Shen W 2014 *IEEE Trans. Electron Dev.* **60** 2104

[12] Mikolasek M, Pribytny P, Donoval D, Marek J, Chvala A, Molnar M and Kovac J 2014 *Appl. Surf. Sci.* **312** 145

[13] Shu Zhan, Das Ujjwal, Allen John, Birkmire Robert and Hegedus Steven 2013 *Progress in Photovoltaic* **23** 78

[14] OlibetS, Vallat-Sauvain E and Ballif C 2007 *Phys. Rev. B* **76** 035326

[15] Li T A, McIntosh K R and Cuevas A 2008 *J. Appl. Phys.* **104** 113718

[16] Garin M, Rau U, Brendle W, Martin I and Alcubilla R 2005 *J. Appl. Phys.* **98** 093711

[17] Shockley W and Read W T 1952 *Phys. Rev.* **87** 835

[18] Hall R N 1952 *Phys. Rev.* **87** 387

[19] Hurkx G A M, Klaasen D B M, Knuvers M P G and Ohara F G 1989 *International Technical Digest on Electron Devices Meeting*, December 3–6, 1989, Washington, DC, USA, p. 30

[20] ATLAS User's Manual, Device Simulation Software, SILVACO, Santa Clara, USA 2016

[21] Gudovskikh A S, Kleider J P, Damon-LascosteJ, Roca iCabarrocas P, Veschetti Y, Muller J C, Ribeyron P J and Rolland E 2006 *Thin Solid Films* **385** 511

[22] Diouf D, Kleider J P and Longeaud C 2012 *Physics and technology of amorphous-crystalline heterostructure silicon solar cells* (New York: Springer) p. 493

[23] Jensen N, Rau U, Hausner R, Uppal S, Oberbeck L, Bergmann R and Werner J 2000 *J. Appl. Phys.* **87** 2639